Progress In Electromagnetics Research M, Vol. 66, 127–142, 2018

Torque Constant Density in Different Type of Double Stator Permanent Magnet Brushless DC Motor

Raja Nor Firdaus Kashfi Raja Othman[1, 2, *], Nor Aishah Md Zuki[1, 2], Suhairi Rizuan Che Ahmad[1, 2, 3], Fairul Azhar Abdul Shukor[1, 2], Siti Zulaika Mat Isa[1, 2], Erwan Sulaiman[4], and Zulkufli Zakaria[5]

Abstract—This paper discusses the torque constant density in different types of Double Stator Permanent Magnet Brushless DC Motor (DSPM) which are designed for portable applications. It should have high torque constant density so that it will have higher torque as well as lightweight. Previously, there have been many DSPM motor designs that only focus on increasing the torque constant and torque density. However, it is unclear which DSPM motor is the best since the torque constant and torque density are different parameters. Torque constant density will include the torque, volume and current of the motor. The objective of this research is to analyze different types of DSPM motors including the proposed Slotted Rotor DSPM motor (DSPM-SR) which produces higher torque constant density. Besides that, this paper also describes in detail the torque constant density from an electromagnetic point of view. Finite Element Analysis (FEA) and analytical calculation are used to simulate the characteristic of various double stators. The result shows that DSPM-SR has 90.5% higher back electromotive force (emf) and 87.5% higher torque than DSPM-ST. Besides that, the DSPM-SR topology has higher torque constant density about 67.27% than other DSPM motors. As a conclusion, this paper provides the overview and comparison of torque constant densities of various DSPM motors.

1. INTRODUCTION

Double stator topology has been recently used in motors for different applications where power segmentation and reliability are the main key factors. The new double stator permanent magnet motor has flexibility as well as high level of precision and system control due to a higher electromagnetic useful torque, compared to a standard permanent magnet synchronous motor [1–3].

In these double stator machines, there are two stator windings which share the same magnetic and mechanical structures. The two windings may have different numbers of poles, phases, and ratings. In double stator machines, the output torque will be higher since currents of both the inner and outer stators produce electromagnetic torque, and two air-gaps can deliver the output torque, thus, improving the torque density [4–6]. Therefore, higher torque can be achieved, and it is suitable for high power applications, in which the double stators produce higher torque density than single stator. Portable applications such as food industries, home appliances, and domestic applications have a strong requirement for a higher torque and small volume which can be indicated by torque density. Torque density, T_d, is defined as the ratio of torque to the volume of the motor. T_d is calculated by using Equation (1).

$$T_d = \frac{T}{V_{ol}} \left[\mathrm{Nm/m^3}\right] \tag{1}$$

Received 23 November 2017, Accepted 6 February 2018, Scheduled 28 March 2018

* Corresponding author: Raja Nor Firdaus Kashfi Raja Othman (norfirdaus@utem.edu.my).

[1] Faculty of Electrical Engineering, Universiti Teknikal Malaysia Melaka (UTeM), Hang Tuah Jaya, Durian Tunggal, Melaka 76100, Malaysia. [2] Electrical Machine Design, Power Electronics and Drives Research Group, CeRIA, UTeM, Hang Tuah Jaya, Durian Tunggal, Melaka 76100, Malaysia. [3] Universiti Kuala Lumpur-British Malaysian Institute, Gombak, Selangor 53100, Malaysia. [4] Universiti Tun Hussein Onn Malaysia, Batu Pahat, Johor, Malaysia. [5] Suria Giant Fan Services Sdn Bhd, Malaysia.

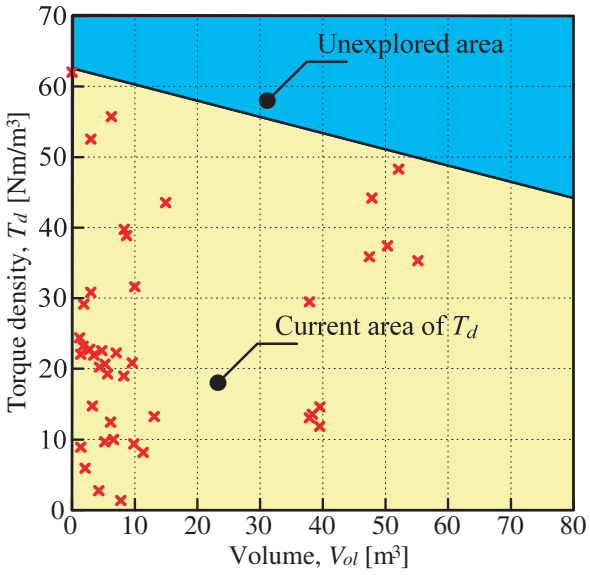

Figure 1. Current reported torque density.

where T is the torque produced by the motor in [Nm], and V_{ol} is the active volume of the motor in [m^3]. The current T_d for Brushless DC Motor (BLDC) available in the market nowadays is shown in Figure 1 as recorded from industrial use and other papers [7–13].

From Figure 1, the highest T_d that was reported is about 62 Nm/m^3. Therefore, T_d beyond this value is an unexplored area. Most studies have focused on T_d at the volume below 100 m^3 due to a higher industrial demand for small volume of motors. Certain applications critically require small size with high torque motor compared to the motor offered by the market. There have been several methods used to increase T_d. Galea et al. found that one way to improve torque density capabilities was by using the outer rotor, CoFe, laminations and open slot [14]. However, it is expensive to use CoFe, making it as one of the main disadvantages of using this approach. Meanwhile, with the use of open slot, it is not possible to achieve a compact and consistent winding layout, and it has high value of slot fill factor, especially if the coils are compacted before assembly.

Another model of BLDC motor known as hollow rotor was proposed before, which has high torque density compared to the conventional spoke motor, but the disadvantage of a single stator is that the optimum efficiency can be achieved only at a certain speed [15]. Chai et al.'s research studied the split ratio between the outer stator and inner stator concluded that a proper matching of the outer and inner split ratios helped to improve the performance of the double-stator motor [16].

Besides torque density, other studies also focus on improving the torque constant, T_c. T_c is defined as the ratio of torque to the value of current as shown in Equation (2).

$$T_c = \frac{T}{I} \text{ [Nm/A]} \tag{2}$$

where I is the input current applied to the motor in [A]. Torque constant, T_c, is related to the flux linkage or inductance. The inductance is affected by winding turn number and reluctance of magnetic circuit [20]. Therefore, T_c indicates the ratio of electrical energy being converted to mechanical energy. The current T_c available in the market is shown in Figure 2 as recorded from industrial use and other papers [17–20]. The highest T_c collected is 6.2 Nm/A. Hence, any value of T_c outside this area is considered an unexplored area.

To increase T_c, Seo et al. found that in order to improve torque constant, a study about pole and slot number of the motor needs to be carried out, as the pole and slot ratio affects the winding factor which is related to torque constant [21]. Therefore, pole and slot number should be determined by considering the manufacturing capabilities, winding factor, and iron loss.

Another research by Park et al. used the estimation technique by calculating the ratio of the back emf to the rotor speed [22]. Besides that, voltage equation is one of the techniques used to obtain

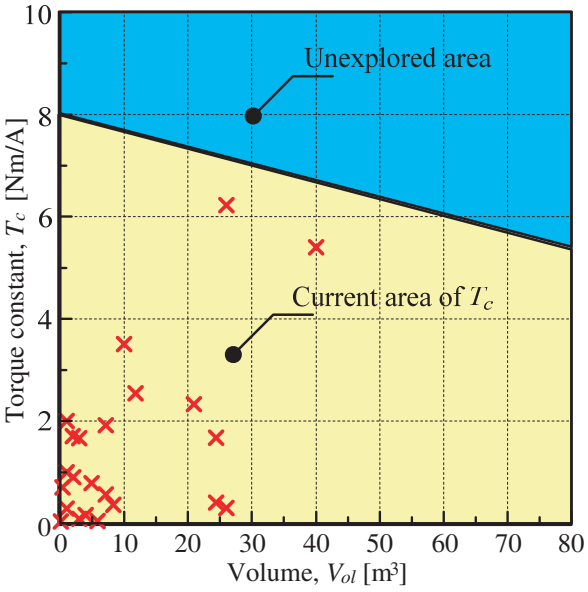

Figure 2. Current reported torque constant.

the torque constant. The rotor position can be obtained by detecting the drop of the estimated torque constant. This method makes it possible to obtain precise position estimation even both in the transient state and in the low-speed range without an external hardware circuit for position detection.

These studies focus on to improve either the torque density or torque constant, but both of the torque density and torque constant have their own weaknesses. T_d is the ratio of mechanical torque over the physical size of motor, while T_c is the ratio of electrical energy (current) being converted to the mechanical energy. Although the double stator motor in the market right now has high T_d and T_c, portable application demands higher T_d and T_c. In order to get a better result, both parameters of T_d and T_c need to be combined as shown in Equation (3).

$$T_{cd} = \frac{T_c}{V_{ol}} \left[\text{Nm/A/m}^3\right] \tag{3}$$

Torque constant density, T_{cd}, is the combination of T_d and T_c. Thus, T_{cd} will consider the mechanical torque, physical size of motor, and also the current injection to the motor. The double stators have high torque because they have two air gaps. Thus, the active current of the two stators induces electromagnetic torque, which is jointly forced on the rotor and output mechanical torque. The double stators have two air gaps so that they have two permeances, and the total torque also will be twice of the single stator [23]. As the air gap becomes smaller, the torque produced will be higher. In order to have a smaller air gap, further research on rotor structure is required so that the permanent magnet can be held, and the stator will not collide with the rotor. Moreover, the rotor structure of double stators in the market is mostly designed as surface mount. For instance, the air gap for a surface mount rotor structure is higher than or equal to 2.0 mm, as there is rotor holder and glue to hold the permanent magnet to ensure no collision with the stator.

Therefore, there are some spaces for these air gaps that can be reduced to achieve the optimum level. In this paper, a new rotor structure known as Slotted Rotor Double Stator Permanent Magnet Motor (DSPM-SR) will have a smaller air gap. At the same time, this DSPM-SR can hold the permanent magnet that makes the rotor more stable and can produce high torque constant density.

For that reason, this paper examines torque constant density for various types of double stators including the proposed DSPM-SR. In this research, various models of DSPM motor in the market are redeveloped, but some of the parameters and the air gap are fixed. Then, the performance of DSPM motor is studied in terms of back emf, torque, and flux linkage. As a result, the DSPM-SR shows the best torque constant density among all DSPM motors. For validation, the DSPM-SR is fabricated and measured experimentally.

2. BASIC STRUCTURE AND PRINCIPLE

2.1. Basic Structure

In this research, 6 types of DSPM motor with different rotor structures will be used, namely Double Stators with Spoke Type Permanent Magnet Motor (DSPM-ST), Double Stator Arc Permanent Magnet Motor (DSPM-AP), Double Stator Double Pole Permanent Magnet Motor (DSPM-DP), Double Stator Interior Permanent Magnet Motor (DSPM-IP), Double Stator Permanent Magnet Motor Cup Rotor (DSPM-CR), and Double Stator Permanent Magnet Motor with Slotted Rotor (DSPM-SR) as shown in Table 1. All DSPM motors have been designed for an arrangement of 18 slots and 20 poles. The type of structure for DSPM motor in this research is designed based on previous studies [19, 24–28]. Some of the DSPM parameters have been fixed specifically. The stator for each model of DSPM motor is made from non-oriented silicon steel. On the other hand, the rotor structure is made from ferromagnetic and non-ferromagnetic material. Besides that, the volumes for all permanent magnets are set at 630 mm^3. Two shapes of permanent magnets, which are arc and rectangular permanent magnets, are used. The stack length and diameter of the motor are 52.5 mm and 156 mm, respectively. Series winding connection is used to coil the outer and inner stators.

Table 1. Fixed parameter for model comparison.

Item	Element	Value
Outer stator	Outer stator diameter	156 mm
Number of turns	Outer stator	55 turns
	Inner stator	55 turns
Number of slots	18	
Number of poles	20	
Number of phase	3	
Permanent magnet volume	$6.3 \times 10^{-7}\,\text{mm}^3$	
Permanent magnet size	6 mm × 2 mm × 52.5 mm	
Coil size	0.7 mm	
Stack length	52.5 mm	
Outer air gap	0.5 mm	
Inner air gap	0.5 mm	
No. of turns of inner coil, N_i	55	
No. of turns of outer coil, N_o	55	

Table 1 shows the fixed parameter to be used for model comparison of DSPM motor such as the diameter of outer stator, the total number of turns for outer and inner stators, the number of slots and poles, number of phases and the air gap between outer and inner stators, stack length, and the total volume of permanent magnet. The total number of turns for all models and the total volume of permanent magnet used are fixed to ensure equal electromagnetic energy by each model. Since the rotor sizes for all models are different, the height of coil in the outer and inner stators varies depending on the rotor structure in order to maintain the mechanical air gap for both inner and outer stators.

Since some of the rotors of DSPM motors are made up from non-ferromagnetic material, the electromagnetic air gap is bigger than the rotors of DSPM motors made from ferromagnetic material, but the mechanical air gaps for all models are fixed which are 0.5 mm for outer and inner stators. It is to ensure that the stator and rotor do not touch each other. Table 2 shows the details of rotor parameter for model comparison of DSPM motors. Each model of DSPM motor has a different size of the outer stator inner radius, r_{osi}, inner stator outer radius, r_{iso}, rotor outer radius, r_{or}, and rotor inner radius, r_{ir}.

Table 2. Parameter of rotor for model comparison.

Model	Element			
	r_{osi} (mm)	r_{iso} (mm)	r_{or} (mm)	r_{ir} (mm)
DSPM-ST	55	44	54.5	44.5
DSPM-AP	58	47.5	57	48.5
DSPM-DP	56	49	55.5	49.5
DSPM-IP	56	47	55.5	47.5
DSPM-CR	58	47.5	57.5	48
DSPM-SR	54	43	53.5	43.5

2.2. Structural Comparison

The detailed views of the DSPM motors are shown in Table 3. Besides that, the explanation for each type of DSPM motor is also discussed in detail. The outer and inner stators for all DSPM motors are made up from ferromagnetic material (Non-oriented silicon steel M250-35A). Figure 3 shows the B-H curve for non-oriented silicon steel M250-35A. The flux density maximum limit or being saturated for this material is about 2 Tesla.

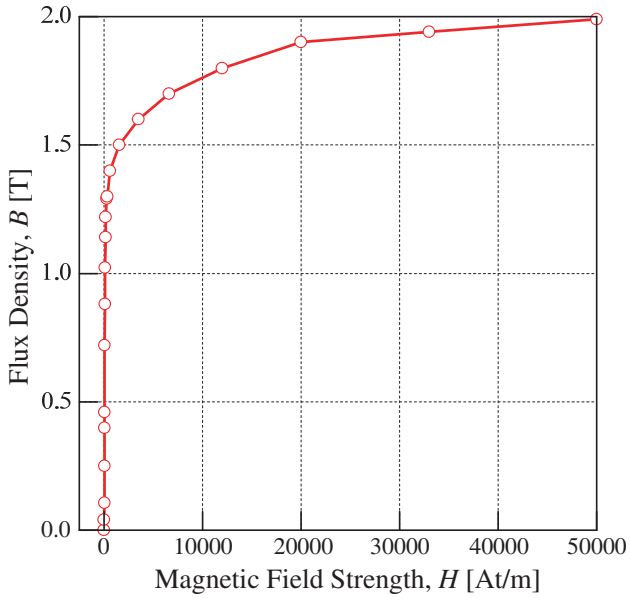

Figure 3. Non-oriented silicon steel M250-35A B-H curve.

2.2.1. Double Stator Spoke Type (DSPM-ST) [24]

Spoke type permanent magnet machine is widely used in industrial applications [23, 24]. The rotor structure of DSPM-ST has a buried type of permanent magnet with higher saliency ratios as shown in Table 3. It means that the magnetic flux generated by permanent magnet arrangement of spoke type is highly concentrated in an air gap and could produce a high power density. The rotor is made up of ferromagnetic material. Here, the flux leakage circling around inside the rotor is compensated by the inner stator. This arrangement has lower cogging torque and is suitable for higher output. However, there is a small percentage of flux leakage circling around the rotor that will affect the output voltage generated.

Table 3. Detailed views of DSPM motors.

	Basic structure	Flux density	Magnetic Equivalent Circuit
DSPM-ST	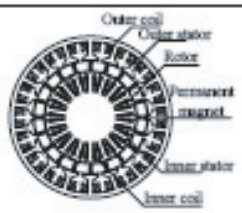	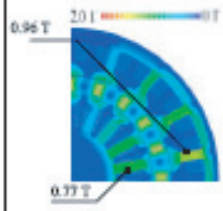	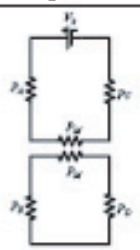
DSPM-AP		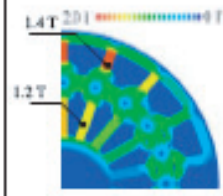	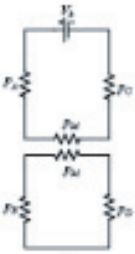
DSPM-DP	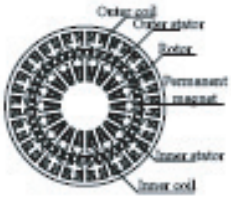	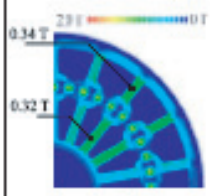	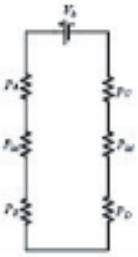
DSPM-IP	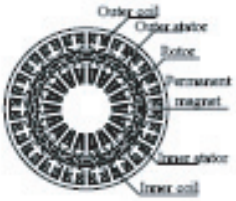	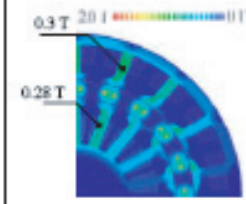	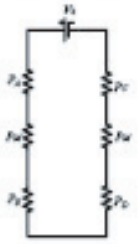
DSPM-CR	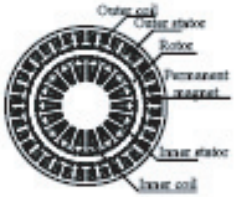	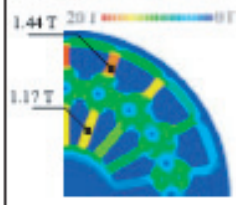	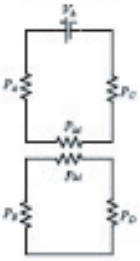
DSPM-SR	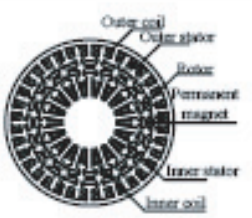	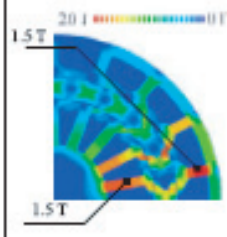	

2.2.2. Double Stator Arc Permanent Magnet (DSPM-AP) [19]

In Table 3, the permanent magnet is designed in arc shape. The permanent magnet is placed at the outer and inner rotor surfaces. Furthermore, there is a gap between the permanent magnet poles. The flux line is circling around the outer stator and inner stator in parallel. This is due to the rotor which is made from ferromagnetic material. Thus, the flux values are different for the outer and inner stators.

2.2.3. Double Stators Double Poles (DSPM-DP) [25]

Detailed view of the basic structure for DSPM-DP is shown in Table 3. The permanent magnets magnetized in circumferential direction are surface-buried in the rotor for high speed application. The magnets are located between wedges of magnetic material of the pole pieces in the rotor. The flux shows that there are two magnets that share the same pole. This is to increase the flux density produced by rotor pole since the rotor is made from non-ferromagnetic material.

2.2.4. Double Stators with Interior Magnet (DSPM-IP) [26]

The basic structure of DSPM-IP is shown in Table 3. In this structure the rotor is made from non-ferromagnetic material. The rotor is cup-shaped with 3.5 mm of total mechanical air gap between permanent magnet and outer and inner stators. The air gap flux density produced by DSPM-IP is lower than 1.0 T due to the non-ferromagnetic material.

2.2.5. Double Stators with Cup Rotor (DSPM-CR) [27]

The basic structure of DSPM-CR is shown in Table 3. The structure of DSPM-CR is identical to that of DSPM-AP, but the permanent magnet is fully mounted on the outer and inner rotor surfaces without any gap. This shows that the flux density produced by DSPM-CR is different for both outer and inner stators as shown in Table 2. The flux line is not fully utilized for both outer and inner stators. Thus, the lowest flux density can be seen at the rotor.

2.2.6. Double Stators with Slotted Rotor (DSPM-SR)

The Double Stator Permanent Magnet Motor with Slotted Rotor (DSPM-SR) introduces permanent magnet embedded inside the rotor. The DSPM-SR can be seen in Table 3. The structure of a slotted rotor will allow a smaller air gap, and at the same time the slotted rotor can hold the permanent magnet that makes the rotor more stable and produce high torque constant density. The flux density produced by DSPM-SR is 1.5 T for both outer and inner stators as shown in Table 3. The flux lines flow from outer to inner stators for a complete path.

3. ANALYTICAL AND NUMERICAL ANALYSIS

Due to model complexity, this research uses the Finite Element Method (FEM). FEM can provide magnetic analysis with high accuracy because it gives an approximation on a microscopic scale. However, it requires structural modeling and high memory capacities of computer, which in the end give more computational time drawbacks. It is clear that the adequacy of meshing directly affects the precision of computation [29–33]. These drawbacks are taken into account in this research to ensure reliability and accuracy. The FEM is used as a tool to obtain the result based on the basic calculation theoretically as below.

The DSPM motor will have two flux linkages which are flux linkage at the outer stator and flux linkage at the inner stator. Therefore, it will also have permeance at the outer stator (P_A and P_C) and permeance at the inner stator (P_B and P_D). However, P_A is equal to P_C, and P_B is equal to P_D. The total flux linkage is the combination of flux linkage at inner stator and flux linkage at the outer stator. In order to calculate the flux linkage of DSPM motor, the total permeance is considered. Since

the other poles are identical, all the calculations are focused on one pole only. Table 3 also shows the magnetic equivalent circuit for each DSPM motor.

$$P_A = \frac{\mu_o l\theta}{\ln\left[1+\frac{g}{r_{ro}}\right]} + 1.63\mu_o\left[r+\frac{g}{4}\right] \text{ [H]} \tag{4}$$

$$P_B = \frac{\mu_o l\theta}{\ln\left[1+\frac{g}{r_{ri}}\right]} + 1.63\mu_o\left[r+\frac{g}{4}\right] \text{ [H]} \tag{5}$$

$$P_M = \frac{\mu w_m l}{2h_m} \text{ [H]} \tag{6}$$

where μ_o is the permeability factor in air in [H/m], μ the permeability in the material in [H/m], θ the angle of the stator in [rad], l the depth of the DSPM in [m], g the air gap between the stator teeth and the rotor in [m], r_{ro} the radius of outer rotor in [m], r_{ri} the radius of inner rotor in [m], r the radius at the air gap in [m], w_m the width of the permanent magnet slot in [m], and h_m the height of the permanent magnet slot in [m]. The total permeance, P_T, for DSPM-ST, DSPM-AP and DSPM-CR is calculated using Equations (7) and (8) meanwhile that for DSPM-DP, DSPM-IP and DSPM-SR is calculated using Equation (9).

$$P_{T1} = \left(\frac{P_A P_M + P_C P_M + P_A P_C}{P_A P_C P_M}\right) \text{ [H]} \tag{7}$$

$$P_{T2} = \left(\frac{P_B P_M + P_D P_M + P_B P_D}{P_B P_D P_M}\right) \text{ [H]} \tag{8}$$

$$P_T = 2\left(\frac{P_A P_M + P_B P_M + P_A P_B}{P_A P_B P_M}\right) \text{ [H]} \tag{9}$$

After the permeance has been obtained, the flux can be calculated. The B-H curve of the permanent magnet and the permeance line of DSSR-BLDC are shown in Figure 4. The operating point of the permanent magnet is at the intersection between these two lines.

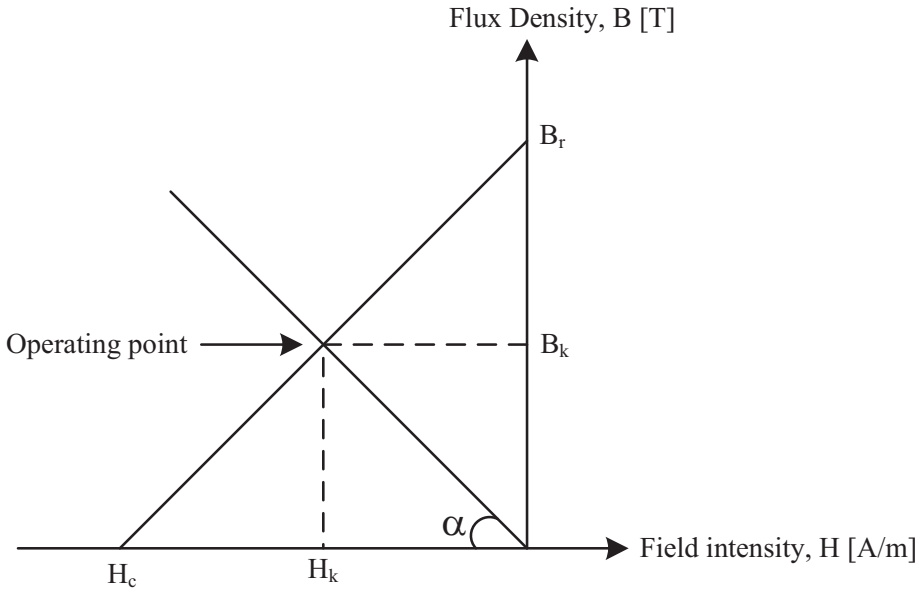

Figure 4. B-H curve and operating point of permanent magnet.

The operating point can be solved by using Equations (10) to (12).

$$\tan\alpha = \frac{P_T H_c h_m}{B_r w_m l} \tag{10}$$

$$B_k = (-\tan\alpha) H_k \,[\mathrm{T}] \tag{11}$$

$$H_k = \frac{-B_r}{\frac{B_r}{H_c} + \tan\alpha} \,[\mathrm{A/m}] \tag{12}$$

where α is the angle of the permeance line slope, P_T the total permeance, H_c the coercive force in [kA/m], B_r a remanent flux density in [T], B_k a magnetic flux density of the permanent magnet at operating point in [T], and H_k the magnetic field intensity of the permanent magnet at operating point in [A/m]. After obtaining the operating point of the permanent magnet, the maximum flux can be calculated by using Equations (13)–(15).

$$\varphi_M = N B_k A_m \,[\mathrm{Wb}] \tag{13}$$

$$\varphi_M = [N][\frac{P_T H_c^2 h_m B_r}{B_r^2 w_m l + P_T H_c h_m}][h_m l] \,[\mathrm{Wb}] \tag{14}$$

$$\varphi_M = \frac{N P_T H_c^2 h_m^2 B_r l}{B_r^2 w_m l + P_T H_c h_m} \,[\mathrm{Wb}] \tag{15}$$

Here, φ_M is the maximum flux at the magnet in [Wb], N the total number of turns in inner and outer stator, A_m the area of the magnet in [m^2], e the electrical degree in [deg], and p the number of poles in DSPM motor. Therefore, the total flux in the DSPM motor is calculated using Equation (19).

$$\varphi = \varphi_M \sin 2\pi \left(\frac{np}{120}\right) + \frac{2e}{p} \,[\mathrm{Wb}] \tag{16}$$

$$W = NI[\varphi_m + \varphi_{coil}] \,[\mathrm{W}] \tag{17}$$

$$\varphi_m = \frac{B_k}{A_m} \,[\mathrm{Wb}] \tag{18}$$

$$\varphi_{coil} = NIP_T \,[\mathrm{Wb}] \tag{19}$$

where W is the co-energy of DSPM motor in [W], N the total number of turns for inner and outer stators, I the current of motor in [A], and φ_{coil} the flux in [Wb]. Finally, the torque equation for permanent magnet motor which can be applied to DSPM motor can be expressed as Equation (20).

$$T_{em} = \frac{mpE_oU}{nX_d} \sin\delta + \frac{mpU^2}{2\omega}\left(\frac{1}{X_q} - \frac{1}{X_d}\right) \sin 2\delta \,[\mathrm{Nm}] \tag{20}$$

where T_{em} is the electromagnetic torque in [Nm], m the number of phases, p the number of pole pair, E_o the back emf in [V], U the applied force in [N], n the motor speed in [rpm]. X_d and X_q are d-axis and q-axis reactances, respectively, and δ is the power angle.

Figure 5 shows the radial flux density. Based on Figure 5, DSPM-AP and DSPM-CR have the highest radial flux density of about 0.55 Wb, This is because the position of magnet is near electromagnetic air gap so that the flux density from the magnet does not have much loss compared to others.

Figure 6 shows the comparison of simulation results for all models under transient mode. Figure 6(a) shows the flux linkage produced by all models of DSPM motor. It clearly suggests that the DSPM-SR produces the highest flux linkage among all models which is 0.15 Wb, while the lowest flux linkage is 0.01 Wb produced by DSPM-ST. The magnetic flux generated by DSPM-ST is highly concentrated at the air gap as shown in Table 3. This is because the air gap is occupied by the rotor pole shoe and stator pole shoe that are made from ferromagnetic material. Based on the result, the flux linkage produced by DSPM-SR is 93.3% higher than DSPM-ST. This is because the flux leakage produced by DSPM-SR is lower than other DSPM motors. The analytical result is almost the same as the simulated one.

Figure 6(b) shows the back emf of each model simulated under various speed conditions. The back emf is directly proportional to the speed. From the result, DSPM-SR produces 90.5% higher back emf

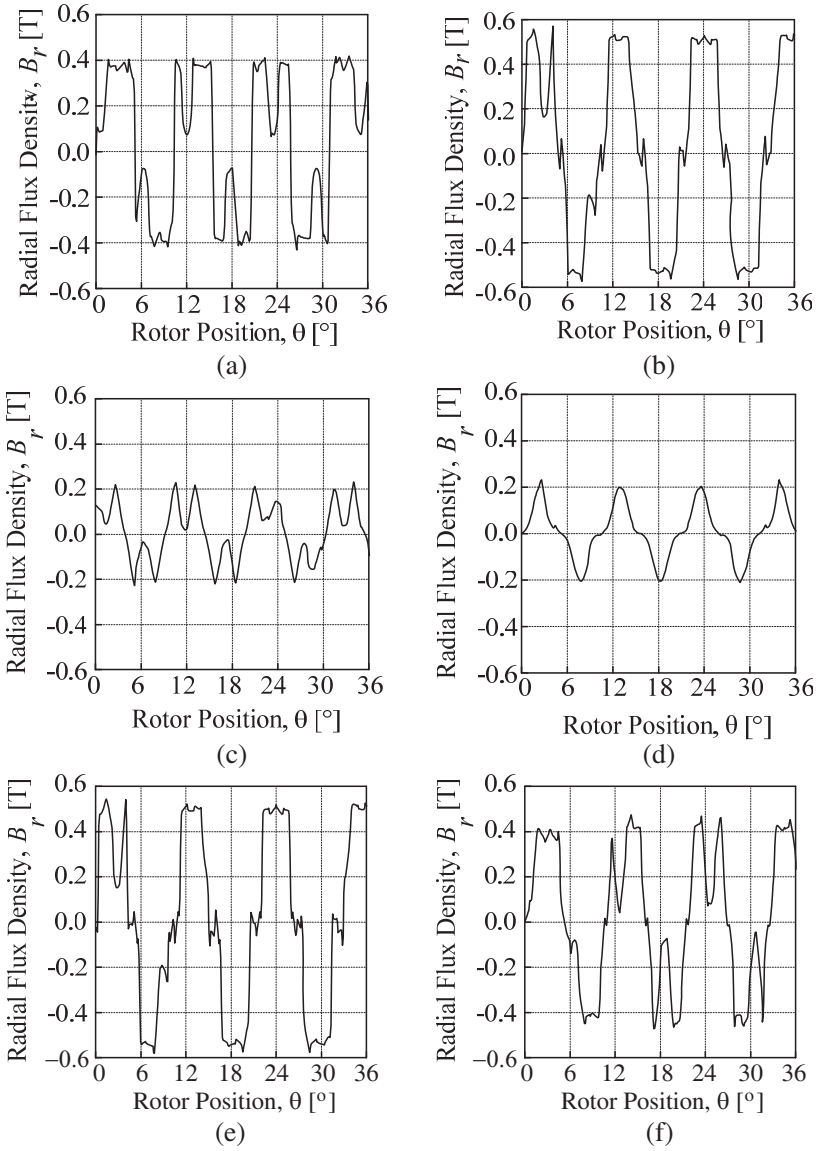

Figure 5. Radial flux density of DSPM motor. (a) DSPM-ST. (b) DSPM-AP. (c) DSPM-DP. (d) DSPM-IP. (e) DSPM-CR. (f) DSPM-SR.

than DSPM-ST. With motor speed of 3500 rpm, DSPM-SR has the highest value of back emf, while the DSPM-ST produces the lowest value, which are 310 V and 29.5 V, respectively.

The DSPM-SR has the highest value of back emf since it has the highest flux linkage among all models as shown in Figure 6(a). Since back emf and flux linkage are related to each other, the analytical result for back emf is also almost identical to the simulation result. Figure 6(c) shows the average torque generated by all models of DSPM motor. The torque is simulated under various current values. At current 6 A, the DSPM-SR produces the highest torque while DSPM-ST gives the lowest value, which are 12.64 Nm and 0.786 Nm, respectively. Thus, the gap percentage between them is 87.5%.

Figure 6(d) shows the comparison result of core loss for all DSPM motors. It indicates that the DSPM-AP and DSPM-CR show the highest core loss, while the DSPM-DP and DSPM-IP show the lowest core loss. This is because the rotor for DSPM-DP and DSPM-IP is made from non-ferromagnetic material. Based on the analysis, the DSPM-SR has the best performance among all the DSPM motors. Thus, DSPM-SR is chosen to be fabricated and goes through the experimental verification.

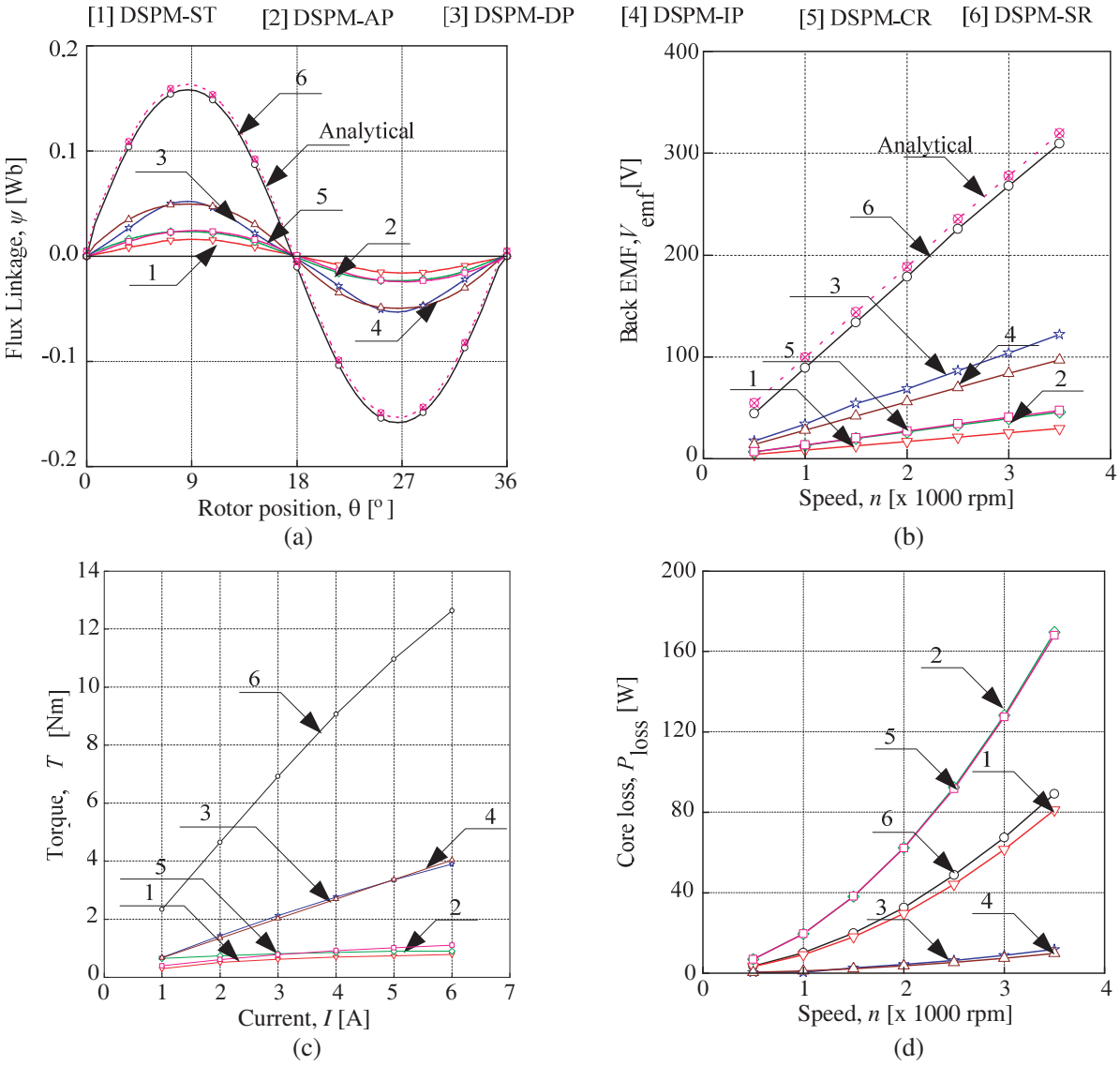

Figure 6. Comparison result for various model of DSPM motor. (a) Flux linkage. (b) Back emf. (c) Torque. (d) Core loss.

4. RESULT AND DISCUSSION

For verification, a prototype of DSPM-SR is fabricated as shown in Figure 7. The experiments are conducted to validate the simulation result. The setup for experimental measurement is shown in Figure 8. The outer stator, inner stator and rotor are each made from non-oriented silicon steel M250-35A with lamination thickness of 0.35 mm while the shaft is made from SUS304 non-carbon. This is for eliminating magnetic flux in the shaft. The permanent magnet used in DSPM-SR is Neodymium Boron Iron (NdFeB42) and placed between the slotted rotor and rotor slots. There are fillers (marked by the yellow colour in Figure 7) made from ABS material. The function of fillers is to provide mechanical strength and prevent the permanent magnet from being displaced from its original position. Besides that, the copper size used is 0.7 mm, and the permanent magnet volume is 630 mm^3. The number of turns in one coil for outer stator is 55, and the number of turns in one coil for inner stator is 55. The total number of turns for both outer and inner stators is 110. The stack length and diameter of DSPM-SR are 52.5 mm and 156 mm, respectively.

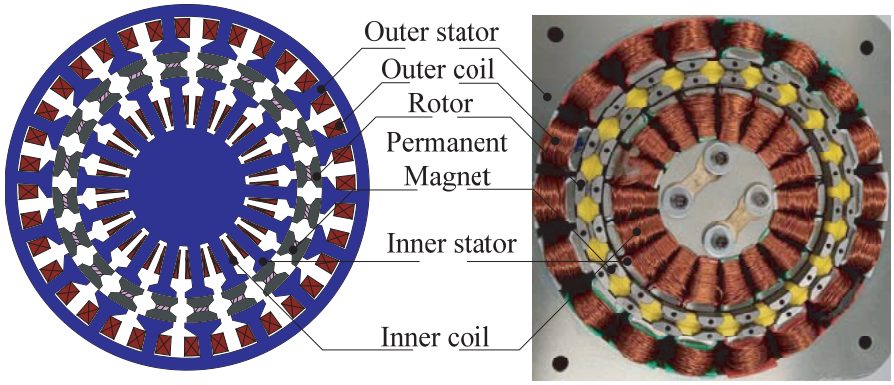

Figure 7. Fabricated DSPM-SR.

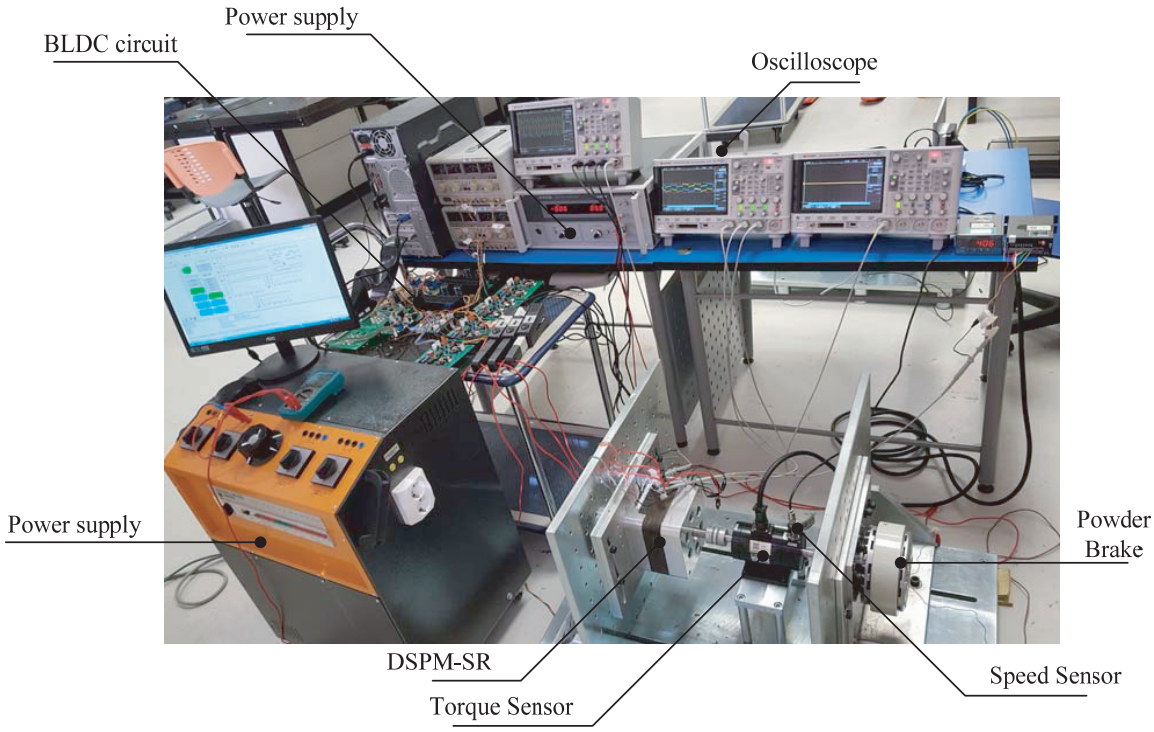

Figure 8. Setup for experimental measurement.

Figure 9 shows the verification result of DSPM-SR. Figure 9(a) shows the back emf of DSPM-SR. This finding indicates that the measurement gives almost identical result to simulation value with only 0.01% difference where, maximum back emf using FEM is 683.34 V, while measurement result is 683.29 V. For measurement result of back emf, a constant speed is given to the motor for recording purpose. Only phase A is compared to FEM simulation and measurement because all three phases have the same pattern.

Dynamic torque is shown in Figure 9(b). The average value of measurement is 2.38 Nm at current 1.3 A, while that from FEM is 2.35 Nm. The average value of dynamic torque from FEM compared to measurement result has a difference of 1.3%. The dotted line shown in Figure 9(c) is T_c for both simulation and measurement. As a conclusion, all results have a good agreement between simulation and measurement.

Table 4 shows the comparative evaluation based on torque constant density, T_{cd}, for all compared

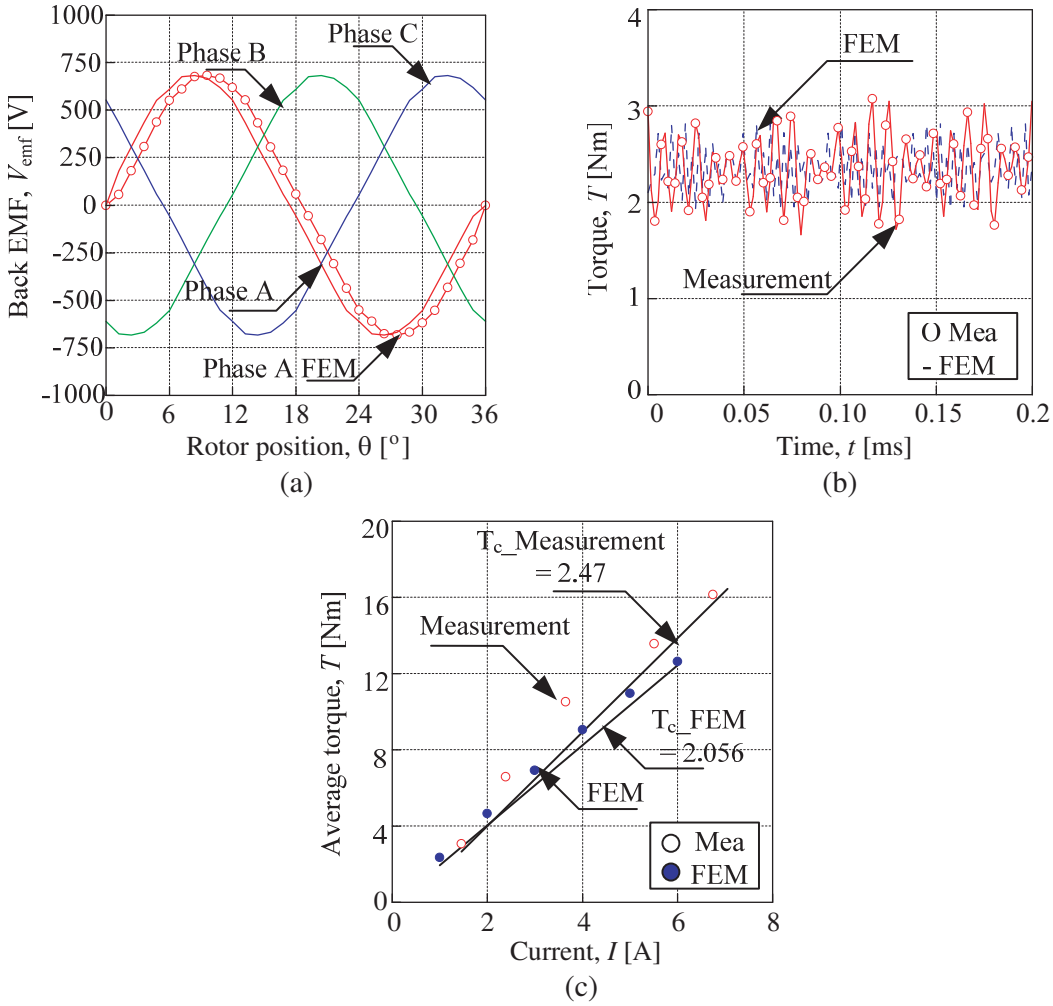

Figure 9. DSPM-SR verification result. (a) Back emf. (b) Torque. (c) Average torque.

Table 4. Torque constant density of DSPM motor.

Model	Parameter							
	I_{max} [A]	V_{ol} [m^3]	T_{c_FEM} [Nm/A]	T_{c_mea} [Nm/A]	T_{d_FEM} [Nm/m^3]	T_{d_mea} [Nm/m^3]	T_{cd_FEM} [Nm/A/m^3]	T_{cd_mea} [Nm/A/m^3]
DSPM-ST	6	1.28×10^{-3}	0.0972	-	234.38	-	75.94	-
DSPM-AP	6	1.28×10^{-3}	0.0486	-	513.13	-	37.97	-
DSPM-DP	6	1.28×10^{-3}	0.6446	-	532.81	-	503.6	-
DSPM-IP	6	1.28×10^{-3}	0.673	-	527.34	-	525.78	-
DSPM-CR	6	1.28×10^{-3}	0.1416	-	310.93	-	110.63	-
DSPM-SR	6	1.28×10^{-3}	2.056	2.47	1830	1866	1606.25	1929.67

models of DSPM motor. The value of torque is obtained from the simulation result. It is found that T_{cd} for DSPM-ST and DSPM-AP are 75.94 Nm/A/m^3 and 37.97 Nm/A/m^3, respectively. Meanwhile, T_{cd} for DSPM-DP, DSPM-IP, DSPM-CR, and DSPM-SR are 503.6 Nm/A/m^3, 525.78 Nm/A/m^3, 110.63 Nm/A/m^3 and 1606.25 Nm/A/m^3, respectively. This shows that DSPM-SR has the highest T_{cd} among all models, and it is the best choice among all motors being studied. Based on the measurement

result, T_{cd} for DSPM-SR is 1929.68 Nm/A/m^3. The difference between simulation and measurement results is 20.14%. The result from FEM has already been considered the core loss but does not account for the friction loss and windage loss.

5. CONCLUSION

In this paper, six types of DSPM motor have been studied in terms of their torque characteristics. These characteristics consist of torque constant T_c, torque density T_d, and torque constant density T_{cd}. Based on the analysis, the proposed DSPM-SR motor shows the highest T_c, T_d as well as T_{cd}. T_c is improved from 0.673 Nm/A to 2.1 Nm/A, and T_d is improved from 1830 Nm/m^3 to 532.81 Nm/m^3, while T_{cd} is improved from 525.78 Nm/A/m^3 to 1606.25 Nm/A/m^3. This shows that DSPM-SR has the highest T_{cd} of about 67.27% among all the DSPM motors. For verification, a prototype of DSPM-SR has been fabricated. In the end, this paper provides understanding on the fundamental of DSPM-SR topology that contributes to high torque constant density.

ACKNOWLEDGMENT

The authors would like to thank the Ministry of Higher Education Malaysia and Universiti Teknikal Malaysia Melaka (UTeM) for providing the research grant of FRGS/1/2015/TK04/FKE/02/F00260, PJP/2016/FKE/H15/ S01478 and GLuar/SURIAGIANT/2017/FKE-Ceria/I00020.

REFERENCES

1. Chai, F., J. Xia, B. Guo, S. Cheng, and J. Zhang, "Double stator permanent magnet synchronous in wheel motor for hybrid electrical drive system," *IEEE Transactions on Magnetic*, Vol. 45, No. 1, 278–281, January 2009.
2. Ho, Z. S., C. M. Uang, P. C. Wang, and S. H. Liu, "Implementation of food processor application using brushless DC motor control," *2011 IEEE Ninth International Conference on Power Electronics and Drive Systems (PEDS)*, 272–277, December 5–8, 2011.
3. Firdaus, R. N., M. Norhisam, N. Mariun, I. Aris, and D. Ahmad, "Torque characteristics of small size single and double stator brushless permanent magnet motor," *IEEE Student Conference on Research and Development*, 52–57, 2011.
4. Dwivedi, A. and R. K. Srivastava, "Analysis of dual stator PM brushless DC motor," *IOSR Journal of Electrical and Electronic Engineering*, Vol. 1, No. 2, 51–56, May–June 2012.
5. Niu, S., K. T. Chau, and J. Z. Jiang, "A permanent-magnet double-stator integrated-starter-generator for hybrid electric vehicles," *IEEE Vehicle Power and Propulsion Conference (VPPC)*, 1–6, September 3–5, 2008.
6. Ahmad, S. R. C., R. N. Firdaus Kashfi Raja Othaman, M. N. Othman, N. A. M. Zuki, F. A. A. Shukor, S. Z. M. Isa, Z. Ibrahim, and C. A. Vaithilingam, "Modeling and analysis of double stator slotted rotor permanent magnet generator," *Energies*, Vol. 10, 1–15, 2017.
7. Firdaus, R. N., N. Misron, C. A. Vaithilingam, M. Nirei, and H. Wakiwaka, "Improvement of energy density in single stator interior permanent magnet using double stator topology," *Research Article*, 1–15, 2014.
8. Hwang, K. Y., S. B. Rhee, B. Y. Yang, and B. I. Kwon, "Rotor pole design in spoke type brushless DC motor by response surface method," *IEEE Transactions on Magnetics*, Vol. 43, 1833–1836, 2007.
9. Lin, D., P. Zhou, and Z. J. Cendes, "Analytical prediction of cogging torque in spoke type permanent magnet motor," *Electrical Machines 2008, ICEM 2008*, 1–5, 2008.
10. Kim, S., J. Cho, S. Park, T. Park, and S. Lim, "Characteristics comparison of a conventional and modified spoke-type ferrite magnet motor for traction drives of low-speed electrical vehicle," *IEEE Energy Conversion Congress and Exposition (ECCE)*, Vol. 49, 2516–2523, 2013.

11. Chen, J. Q., G. Liu, W. Zhou, and M. Shou, "Nonlinear adaptive lumped parameter magnetic circuit analysis for spoke-type fault-tolerant permanent magnet motors," *IEEE Transactions on Magnetics*, Vol. 49, 5150–5157, 2013.
12. Kim, D. Y., J. K. Nam, and G. H. Jang, "Reduction of magnetically induced vibration of a spoke-type IPM motor using magneto mechanical coupled analysis and optimization," *IEEE Transactions on Magnetics*, Vol. 49, 5097–5105, 2013.
13. Sinotech (2014) Brushless DC Motor (BLDC) Retrieved from http://www.sinotech.com/.
14. Galea, M., T. Hamiti, and C. Gerada, "Torque density improvement for high performance machines," *2013 IEEE International Electric Machines & Drives Conference (IEMDC)*, 1066–1073, 2013.
15. Firdaus, R. N., R. Suhairi, S. Farina, K. A. Karim, and Z. Ibrahim, "Improvement of power density spoke type permanent magnet generator," *IEEE PEDS 2015*, 197–201, 2015.
16. Chai, F., J. Xia, H. Gong, B. Guo, and S. Cheng, "Torque analysis of double stator permanent magnet synchronous for hybrid electric vehicle," *2008 IEEE Vehicle Power and Propulsion Conference (VPPC)*, 1–5, 2008.
17. Mihail-Florin, S., C. Cosmin, F. Nicolae, and H. Adela-Gabriela, "A variant of a synchronous motor with two stators and high-energy permanent magnets disposed on the both rotor peripheries," *ECAI 2015 International Conference on Electronics*, 9–14, 2015.
18. Niu, S., K. T. Chau, D. Zhang, J. Z. Jiang, and Z. Wang, "Design and control of a double-stator permanent magnet motor drive for electric vehicles," *IEEE Industry Application Conference*, Vol. 25, No. 18, 1293–1300, 2007.
19. Niu, S. and L. Jian, "Scalar control of double-stator permanent magnet brushless motor drives," *2009 International Conference on Power Electronics and Drive Systems (PEDS)*, 354–359, 2009.
20. Wang, Y., M. Cheng, Y. Du, and S. Ding, "Vector control of double-stator permanent magnet brushless motor with surface mounted topology," *2010 International Conference on Electrical Machines and Systems (ICEMS)*, 855–858, 2010.
21. Seo, J.-M., J.-H. Kim, S.-H. Rhyu, J.-H. Choi, and I.-S. Jung, "A study on brushless DC motor for high torque density," *International Journal of Mechanical, Aerospace, Industrial, Mechatronic and Manufacturing Engineering*, Vol. 5, 2084–2088, 2011.
22. Park, J.-W., S.-H. Hwang, and J.-M. Kim, "Sensorless control of brushless DC motors with torque constant estimation for home appliances," *IEEE Transactions on Industry Applications*, Vol. 40, 677–684, 2012.
23. Vaithilingam, C. A., N. Misron, I. Aris, M. H. Marhaban, and M. Nirei, "Electromagnetic design and FEM analysis of a novel dual-air reluctance machine," *Progress In Electromagnetic Research*, Vol. 140, 523–544, 2013.
24. Chai, F., S. Cui, and C. Kang, "Performance analysis of double-stator starter generator for the hybrid electric vehicle," *2004 12th Symposium on Electromagnetic Launch Technology*, 499–502, 2015.
25. Kim, S.-I., J. Cho, S. Park, T. Park, and S. Lim, "Characteristics comparison of a conventional and modified spoke-type ferrite magnet motor for traction drives of low-speed electric vehicles," *IEEE Transactions on Industry Applications*, Vol. 49, 2516–2523, 2013.
26. Kim, K.-C. and J. Lee, "The dynamic analysis of a spoke-type permanent magnet generator with large overhang," *IEEE Transactions on Magnetics*, Vol. 41, 3805–3807, 2005.
27. Norhisam, M., M. Norafiza, and C. Y. Sia, "Double stator type permanent magnet generator," *Proceeding of 2009 Student Conference on Research and Development (SCOReD 2009)*, 316–319, UPM Serdang Malaysia, November 16–18, 2009.
28. Wang, Y., M. Cheng, Y. Fan, and K. T. Chau, "A double-stator permanent magnet brushless machine system for electric variable transmission in hybrid electric vehicles," *2010 IEEE Vehicle Power and Propulsion Conference*, 1–5, 2010.

29. Chai, F., J. Xia, B. Guo, and S. Cheng, "Double-stator permanent magnet synchronous in-wheel motor for hybrid electric drive system," *2008 14th Symposium on Electromagnetic Launch Technology*, 1–5, 2008.
30. Firdaus, R. N., M. Norhisam, I. Aris, M. Nirei, and H. Wakiwaka, "Analysis on harmonics components of torque characteristics of single phase single stator small size brushless DC permanent magnet motor," *International Review of Electrical Engineering*, 5413–5424, 2012.
31. Hirata, K., Y. Kagami, M. Yanosaka, Y. Ishihari, and T. Todaka, "Thrust calculation of linear pulse motors using a combined technique employing the finite element and the permeance analysis method," *IEEE Transactions on Magnetics*, Vol. 28, No. 2, 1394–1397, 1992.
32. Delforge, C. and B. Lemaire-Semail, "Induction machine modeling using finite element and permeance network methods," *IEEE Transactions on Magnetics*, Vol. 31, No. 3, 2092–2095, 1995.
33. Wang, X., Q. Li, S. Wang, and Q. Li, "Analytical calculation of air-gap magnetic field distribution and instantaneous characteristics of brushless DC motors," *IEEE Transactions on Energy Conversion*, Vol. 18, No. 3, 424–432, 2002.